

A STATISTICAL TOMOGRAPHIC APPROACH TO SYNTHETIC APERTURE RADAR IMAGE RECONSTRUCTION *

Müjdat Çetin and William C. Karl

Multi-Dimensional Signal Processing Laboratory
Department of Electrical and Computer Engineering
Boston University
8 Saint Mary's Street, Boston, MA 02215, USA

ABSTRACT

We formulate the spotlight-mode synthetic aperture radar (SAR) imaging problem as a maximum a posteriori (MAP) estimation problem. Our statistical perspective offers an alternative to standard SAR processing techniques by incorporating prior knowledge about either the data quality or the underlying reflectivity function. In our formulation we consider exploiting the similarity between computer assisted tomography (CAT) and spotlight-mode SAR, which was first exposed by Munson et al. [1]. We present the effectiveness of the proposed approach by imagery formed from simulated spotlight-mode SAR data.

1. INTRODUCTION

The objective of spotlight-mode SAR imaging is to synthesize high-resolution images using data collected at multiple observation points. The spotlight-mode SAR observation kernel consists of a band-limited Fourier transformation of the reflectivity field to be imaged. As a consequence of this, and owing to its computational efficiency, the standard image formation algorithm has been the two-dimensional fast Fourier transformation (FFT).

Munson et al. [1] have observed that spotlight-mode SAR can be considered as a narrow-band version of CAT. Since that time, use of this significant insight for the processing of SAR data appears to have been largely limited to the application of the CAT filtered backprojection (FBP) algorithm to the reconstruction of SAR returns, as in [2]. The close relationship between SAR and CAT suggests other SAR data processing and analysis approaches, however. We aim to exploit this similarity in various SAR information processing tasks. In this paper in particular, we explore the use of the tomographic formulation of the spotlight-

mode SAR data relationship as the basis for alternative algorithms for SAR data inversion and high resolution image formation. Previously Lee et al. [3] have applied a regularized inversion method for strip-mapping SAR. In [4], Borden has used maximum entropy regularization for inverse synthetic aperture radar (ISAR) image formation. Our work includes explicit use of an accurate tomographic forward model for spotlight-mode SAR data collection and casting of the image formation problem as a MAP estimation problem.

2. SPOTLIGHT-MODE SAR OBSERVATION MODEL

Consider the ground plane geometry in Figure 1 for spotlight-mode SAR. Data are collected by a radar traversing a flight path and continuously pointing in the direction of the ground patch to be imaged. We will assume that the flight path is linear. At points corresponding to equal angular increments, high-bandwidth pulses are transmitted and returns from the ground patch are then received and processed. In this paper we will make a typical assumption that linear FM chirp signals are transmitted by the radar. The objective of SAR image formation is to form an image of the complex reflectivity field from the measured signals. Let us assume the radar transmits a pulse at angle θ . After multiplying the return signal from the scene with a reference chirp signal and low-pass filtering, the phase from a unit reflectivity point scatterer at a specified location is given by

$$\phi_{\theta}(t) = -j\frac{2}{c} \left[w_0 + 2\alpha(t - \frac{2R_0}{c}) \right] u \quad (1)$$

where a quadratic phase term has been neglected [5]. Here R_0 is the instantaneous range to the patch center, u is the difference between the instantaneous range to the point target and R_0 , c is the speed of light, w_0 is the radar FM chirp carrier frequency and 2α is the chirp rate. Now let $p_{\theta}(u)$ be the sum of complex reflectivities

*This work was supported by the Air Force Office of Scientific Research under Grant F49620-96-1-0028.

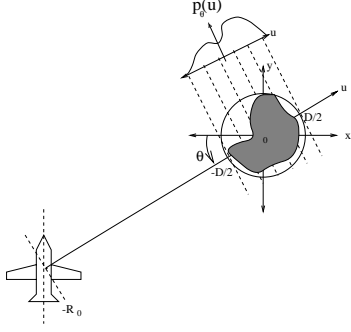


Figure 1: Ground plane geometry and projectional data collection in spotlight-mode SAR.

of all point targets that are equidistant from the radar at a particular transmission angle θ . If we assume that the curvature of the wavefront is negligible, the return signal from the circular patch of diameter D is given by [1]

$$r_\theta(t) = \int_{-D/2}^{D/2} p_\theta(u) \exp \left\{ -j \frac{2}{c} \left(w_0 + 2\alpha \left(t - \frac{2R_0}{c} \right) \right) u \right\} du \quad (2)$$

which is nonzero for $-\frac{\tau}{2} + \frac{2(R_0+D/2)}{c} \leq t \leq \frac{\tau}{2} + \frac{2(R_0-D/2)}{c}$, where τ is the transmitted pulse duration. Thus our observations $r_\theta(t)$ are intimately related to the projections $p_\theta(u)$ of the desired underlying field, as is also the case in CAT. In particular, this signal can be identified as the Fourier transform of the projection $p_\theta(u)$ where the spatial frequency variable is $\frac{2}{c}(w_0 + 2\alpha(t - \frac{2R_0}{c}))$. Since the observation duration t is limited, the spatial frequency is also limited to a finite interval. After collecting returns from all transmission points (i.e. all angles), the resulting data can be identified as the 2-D Fourier transform of the reflectivity field confined to an annular region in the frequency domain, whose displacement from the origin is determined by w_0 and whose size is determined by the range of look angles and the bandwidth ($2\alpha\tau$) of the transmitted radar signal. Observing projectional information at a high frequency rather than at the baseband is the key behind our ability to obtain high cross-range resolution in SAR with a range of look angles of only a few degrees [6].

We can write (2) more compactly as $r_\theta(t) = (\mathcal{F}_L p_\theta)(u)$ where \mathcal{F}_L is the band-limited Fourier transform kernel. Letting $f(x, y)$ be the underlying reflectivity field, we also have $p_\theta(u) = (\mathcal{T}_\theta f)(x, y)$, where \mathcal{T}_θ is the projection operator, taking line integrals along the dotted lines in Figure 1. Now we can write the relationship between our observations and the unknown reflectivity field as $r_\theta(t) = (\mathcal{C}_\theta f)(x, y)$, where $\mathcal{C}_\theta = \mathcal{F}_L \mathcal{T}_\theta$.

In practice the observations $r_\theta(t)$ are sampled. This sampling in the time domain results in sampling of the spectrum of the underlying reflectivity field. Sampling places a limit on the maximum allowable scene size that can be imaged without aliasing (in the spatial domain).

Letting r_θ be the observation vector consisting of the collection of samples of $r_\theta(t)$, C_θ be a discretized approximation to \mathcal{C}_θ , and f be the unknown sampled reflectivity image column stacked as a vector, we can write

$$\underbrace{\begin{bmatrix} r_{\theta_1} \\ r_{\theta_2} \\ \vdots \\ r_{\theta_N} \end{bmatrix}}_r = \underbrace{\begin{bmatrix} C_{\theta_1} \\ C_{\theta_2} \\ \vdots \\ C_{\theta_N} \end{bmatrix}}_C \underbrace{f}_f \quad (3)$$

where N is the total number of angular observation points. Since each $r_\theta(t)$ is a band-pass filtered Fourier transform of the projection $p_\theta(u)$, we can get samples of a finite resolution reconstruction of the projectional information by an inverse discrete Fourier transformation (DFT) of the sampled data at each observation angle. Let $\bar{p} = F^{-1}r$ be the collection of the samples of these band-pass filtered projections at all angles, column stacked as a vector. Here F is the matrix performing a DFT at each observation angle. We can now write the following projectional data relationship

$$\bar{p} = T_{\text{SAR}} f \quad (4)$$

where $T_{\text{SAR}} = F^{-1}C$ represents a discrete ‘‘SAR projection operator’’.

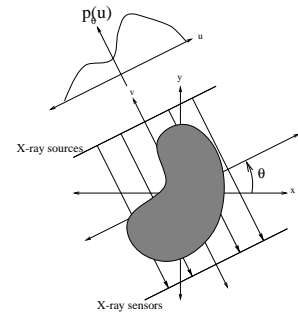


Figure 2: Data collection geometry in CAT.

SAR projections are in general complex-valued as opposed to the real-valued projections recording attenuation in CAT, as shown in Figure 2. The similarity of

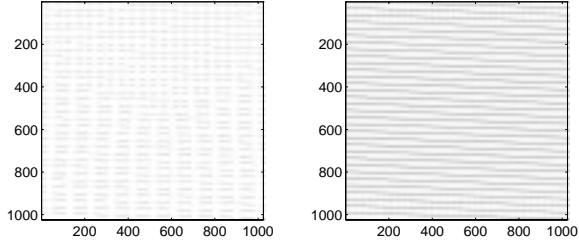


Figure 3: The grayscale plot (black corresponds to the maximum value and white to the minimum) of the magnitude of elements in the projection matrices for CAT (left) and SAR (right).

the structure of the discrete CAT and SAR projection operators for a typical SAR data collection geometry is shown in Figure 3. The images in this figure are grayscale plots of the magnitudes of elements of the corresponding projection matrices. Here an underlying field of 32×32 pixels, and projectional data of length 32 at each of 32 angular observation points have been assumed.

3. SAR IMAGE RECONSTRUCTION

The conventional approach to SAR image formation is to interpolate the collected samples of the 2-D spectrum from the polar grid to a rectangular one and then take the 2-D inverse FFT to form the image. Another image reconstruction method, suggested by the tomographic formulation, is the FBP algorithm. In this method, data at each observation angle is filtered by a suitable ramp filter, and then backprojected to obtain a reconstruction.

Neither of these approaches allow the inclusion of prior information about either the data quality or the underlying reflectivity function itself, and hence they are sensitive to incomplete or noisy observations, which in turn might cause undesired artifacts in the image. For this reason we take a statistical perspective and seek a reconstructed reflectivity field as the solution to a MAP estimation problem. We model our noisy observations of the sampled field as

$$g = r + w = Cf + w \quad (5)$$

where w is Gaussian zero mean noise with covariance R . We form C by calculating the sampled phase history corresponding to point targets in the scene by using (1) for all the observation points. The assumed number of point reflectors in the underlying field, equivalently, the pixel spacing in the reconstructed image determines the size of f . We assume that the unknown reflectivity field has a prior Gaussian distribution with zero mean and covariance Q .

carrier frequency (w_0)	$2\pi \times 10^{10}$ rad/s.
chirp rate (2α)	$2\pi \times 10^{12}$ rad/s ² .
pulse duration (T)	4×10^{-4} sec.
patch diameter (D)	12 m.
angular range ($\Delta\theta$)	2.3 deg.

Table 1: SAR system parameters used in the examples.

We then form the estimate of the reflectivity field as the MAP estimate:

$$\begin{aligned} \hat{f}_{MAP} &= \arg \max_f [p_{f|g}(f|g)] \\ &= \arg \min_f [\|g - Cf\|_{R^{-1}}^2 + \|f\|_{Q^{-1}}^2]. \quad (6) \end{aligned}$$

4. RESULTS

We have simulated a spotlight-mode SAR system with the parameter values illustrated in Table 1. With these parameters the bandwidth of the transmitted signal is 0.4 GHz, implying a range resolution of 0.375 m. We choose to set the azimuth resolution equal to the range resolution, which requires an angular observation interval of 2.3 degrees. The angular measurements are taken symmetrically around $\theta = 0$ degrees. We assume the imaged ground patch to have a diameter of 12 m. In a real system, the imaged region is usually much larger, the reason behind keeping it small here is to reduce the computational complexity. The data sampling rate should be chosen according to $f_s \geq 2D\alpha/(\pi c)$ to prevent aliasing in the reconstructed image.

As a first example we will consider a simple scenario and demonstrate point target reconstructions. For this example, we use simulated SAR data obtained by generating the phase history corresponding to three point targets with unit reflectivity magnitude at coordinates $(-3.1875, -0.1875)$, $(-0.1875, -0.1875)$ and $(-0.1875, -3.1875)$ with respect to a coordinate system centered at the patch center. The elements in each pair denote the range and cross-range displacements (in meters) respectively. The real and imaginary parts of the observations are then contaminated with zero mean independent identically distributed Gaussian noise such that the signal to noise ratio (SNR) is 5 dB. Our reconstruction model for this example uses $R = 0.46I$ and $Q = 0.003I$. Thus our prior model assumes the unknown reflectivity field is composed of independent identically distributed Gaussian random variables. The result illustrated in Figure 4 suggests our approach possesses good target localization in this limited angle configuration.

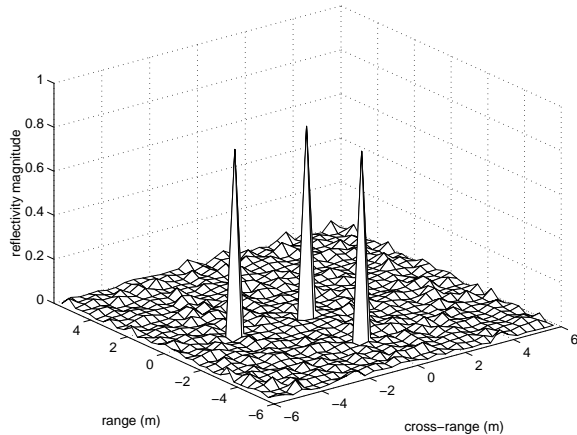


Figure 4: MAP estimate of the scene composed of three point targets (SNR = 5 dB).

Next we compare our results with the standard methods on a more realistic SAR scene. In Figure 5 we show magnitudes of reconstructed images of a scene containing a military target. Here no noise is added to the data samples. The images formed by all the three methods; the FFT, the FBP and the MAP, seem to be acceptable reconstructions. The MAP solution however is smoother than the other two. This is due to our prior model assumption for the field. Here we assume a fractal-type prior with Q^{-1} equal to a discrete approximation of the Laplacian operator.

Finally we will demonstrate the use of prior information about data quality. In this example we add independent identically distributed Gaussian noise to the data samples such that the SNR is 8 dB. The reconstructions obtained by the three methods are illustrated in Figure 6. The FFT and the FBP algorithms cannot produce intelligible reconstructions due to their sensitivity to noise. The MAP estimate however is robust enough to produce a reasonable reconstruction in this low SNR scenario.

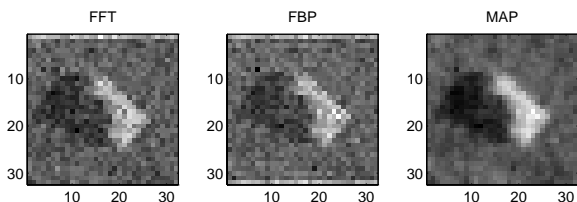


Figure 5: Reconstructions with high quality data.

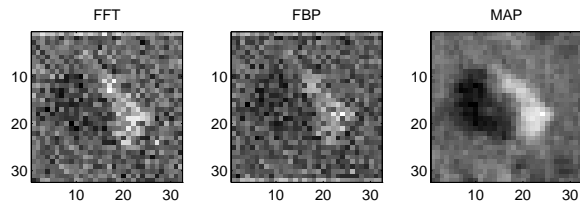


Figure 6: Reconstructions with low quality data.

5. CONCLUSION

We have formulated the spotlight-mode SAR imaging problem in a statistical framework, using a tomographic data acquisition model. Our approach offers an alternative to conventional SAR image reconstruction methods with enhanced noise suppression and artifact reduction properties. The solutions generated by our method however require much more computation than the standard methods. The development of computationally tractable solution methods is a topic of current research.

6. REFERENCES

- [1] D. C. Munson Jr., J. D. O'Brien, and W. K. Jenkins, "A tomographic formulation of spotlight-mode synthetic aperture radar," *Proc. IEEE*, vol. 71, pp. 917-925, Aug. 1983.
- [2] M. D. Desai and W. K. Jenkins, "Convolution back-projection image reconstruction for spotlight mode synthetic aperture radar," *IEEE Trans. Image Processing*, vol. 1, no. 4, pp. 505-517, Oct. 1992.
- [3] J. A. C. Lee and D. C. Munson Jr., "Formulation of a general imaging algorithm for high-resolution synthetic aperture radar," *Proceedings of the 1996 IEEE International Conference on Acoustics, Speech and Signal Processing*, pp. 2094-2099, Sept. 1996.
- [4] B. Borden, "Maximum entropy regularization in inverse synthetic aperture radar imagery," *IEEE Trans. Signal Processing*, vol. 40, no. 4, pp. 969-973, Apr. 1992.
- [5] C. V. Jakowatz Jr., D. E. Wahl, P. H. Eichel, D. C. Ghiglia and P. A. Thompson, *Spotlight-mode synthetic Aperture Radar: a Signal Processing Approach*, Kluwer Academic Publishers, 1996.
- [6] A. Di Cenzo, "A comparison of resolution for spotlight synthetic-aperture radar and computer-aided tomography," *Proc. IEEE*, vol. 74, pp. 1165-1166, Aug. 1986.